JOURNAL OF Materials CHEMISTRY

Templated electrochemical deposition of nanostructured macroporous PbO_2

Philip N. Bartlett,* Tim Dunford and Mohamed A. Ghanem

Department of Chemistry, University of Southampton, Highfield, Southampton, UK SO17 1BJ

Received 31st May 2002, Accepted 4th July 2002
First published as an Advance Article on the web 12th August 2002

We report a simple method for the preparation of novel nanostructured macroporous α- and β-PbO_2 films with arrays of spherical pores arranged in a highly ordered close-packed structure. The nanostructured macroporous α- and β-PbO_2 films were prepared by electrochemical deposition through the interstitial spaces between polystyrene spheres (500 or 750 nm in diameter) assembled on gold or indium tin oxide substrates. After deposition, the template was removed by dissolving in toluene to leave PbO_2 films that have the inverse structure of the original template. Scanning electron microscopy and X-ray characterisation of the films shows a well-formed regular three-dimensional, porous α- or β-PbO_2 framework, with the spherical pores arranged in a highly ordered close-packed three-dimensional structure. The spherical pores have the same diameter as the latex spheres used to form the templates and are interconnected through a series of smaller pores. The oxide frameworks are highly polycrystalline, self-supporting and free from defects. The confinement of α-PbO_2 and β-PbO_2 in the interstitial spaces between the polystyrene spheres that make up the template does not affect the mechanism of nucleation and deposition or the crystal structure of the oxide, as confirmed by scanning electron microscopy and X-ray characterisation. The electrochemical activity of the resulting macroporous β-PbO_2 is greater than that of the corresponding plain film, as determined by the charge passed to convert the β-PbO_2 to $PbSO_4$ on electrochemical cycling in H_2SO_4. Due to the increase in volume accompanying the electrochemical conversion of β-PbO_2 to $PbSO_4$, the macroporosity of the film is significantly degraded and the electrochemical activity decreased after a few cycles in sulfuric acid.

Introduction

Macroporous metal oxides (pore diameters $\geqslant$ 50 nm) have been used as filtration and separation materials,[1] catalyst supports,[2] battery materials,[3] and as photonic materials.[4] Recently developed colloidal crystal-templated synthesis techniques have enabled the chemical preparation of macroporous metal oxides with three-dimensionally ordered arrays of regular, sub-micron diameter pores.[5–7] Nanostructured macroporous oxides of Si, Ti, Zr, Al and Fe have all been obtained by filling the space between close-packed arrays of polystyrene or silica spheres with a precursor solution, which is then chemically or thermally transformed to a solid oxide skeleton around the spheres. Although the use of chemical or thermal methods for the synthesis of macroporous metal oxides leads to the formation of three-dimensional macroporous close-packed structures, these methods suffer the disadvantages of filling defects (discontinuities), the considerable shrinkage of the structures (by up to 30%), as well as problems of contamination during the chemical reduction of the metal salt or calcination processes.[4,5,8,9]

Electrochemical deposition has also been applied to colloidal template-directed synthesis of semiconductors,[10] metals[11–13] and conducting polymers.[14,15] Electrochemical deposition through colloidal crystal templates has a number of significant advantages as a method for preparing this type of macroporous material, particularly for the deposition of thin, supported films. Electrochemical deposition ensures a high density of the deposited material within the space between the template spheres and leads to true "volume templating" of the structure, rather than surface templating of material around the surface of the template spheres. As a result, there is no shrinkage of the material when the template is removed and no need for further processing steps or the use of elevated temperatures. In consequence, the resulting porous film is a true cast of the template structure and the size of the spherical pores within the film is directly determined by the size of the template spheres used. The method also has flexibility in the choice of materials which can be used, since there are a large number of oxides, metals, alloys, semiconductors and conducting polymers which can be electrochemically deposited, both from aqueous and non-aqueous solutions, under conditions which are compatible with the template. Finally, the use of electrochemical deposition allows direct control over the thickness through control of the charge passed to deposit the film. This is a unique feature of the approach.

It is also important to note that, because the template spheres are assembled onto the flat surface of the electrode and because electrochemical deposition occurs from the electrode surface out through the overlying template, the first layer of templated material, deposited out to a thickness comparable to the diameter of the template spheres used, has a different pore structure from subsequent layers. Further growth of the film by electrodeposition out through the template leads to a modulation of the surface topography of the film in a regular manner that depends on the precise choice of deposition bath and deposition conditions.[16]

Despite these advantages, to the best of our knowledge there are only two papers that describe the electrochemical deposition of a macroporous metal oxide film. Sumida *et al.*[17,18] reported the electrochemical deposition of ordered macroporous ZnO and WO_3 films by electrochemical deposition through templates of polystyrene colloidal crystals. The resulting films have an inverse opal macroporous structure.

Lead dioxide has a wide range of important uses. Most well known is its use as the positive electrode in lead acid batteries and the stability of PbO_2 in acidic media makes it ideal for this application.[19] In addition, PbO_2 can be used as an electrode in the electro-oxidation of organic and inorganic materials,[20,21] ozone generation[22] and in oxidative degradation

 DOI: 10.1039/b205306c

of organic pollutants such as dimethylsulfoxide[23] and phenols.[24,25] In the literature, lead nitrate and lead acetate solutions have been used for the electrochemical deposition of lead dioxide films.[26,27] Two different crystalline phases of lead dioxide can be obtained depending on the conditions used: tetragonal β-PbO_2 is obtained from acidic electrolyte, whereas the orthorhombic α-PbO_2 can be deposited from basic and neutral electrolytes.[28–30]

In this paper, we describe the templated deposition of thin macroporous films of both α-PbO_2 and β-PbO_2 by electrochemical deposition within the interstitial spaces between close-packed polystyrene spheres (500 or 750 nm in diameter). The resulting macroporous films were examined by scanning electron microscopy and X-ray diffraction. In addition, we have measured the electrochemical activity of macroporous β-PbO_2 in sulfuric acid.

Experimental

Materials and substrates

Monodisperse polystyrene latex spheres, with diameters of 500 and 750 ± 20 nm, were obtained from Alfa Asear as 2.5 wt% solutions in water. Lead acetate (purity 99.8%), lead nitrate (purity 99.9%), and sodium acetate were obtained from Aldrich. Propanol, sulfuric acid (Analar grade > 98%) and toluene were obtained from BDH. All other solvents and chemicals were of reagent quality and were used without further purification. All solutions were freshly prepared using reagent grade water (18 MΩ cm) from a Whatman RO80 system coupled to a Whatman "Still Plus" system. The gold electrodes used as substrates were prepared by evaporating 10 nm of a chromium adhesion layer, followed by 200 nm of gold, onto 1 mm thick glass microscope slides. The indium tin oxide (ITO) substrate was obtained from Sheldahl. Both gold and ITO substrate were cleaned by sonication in propanol for 1 h followed by rinsing with deionised water.

Instrumentation

Electrochemical deposition was carried out in a conventional three-electrode configuration using an EG&G 273A instrument. A large area platinum gauze was used as the counter electrode with a home-made saturated calomel (SCE) reference electrode with the template-coated substrate as the working electrode. Analytical scanning electron microscopy (JEOL 6400 or Philips XL30ESEM) and X-ray diffractometry (Siemens Diffraktometer D5000 using Cu-Kα radiation) were employed to study the morphology and microstructure of the oxide films.

Assembly of the colloidal templates

The polystyrene sphere templates were assembled by sticking a 1.0 cm internal diameter Teflon ring on to the substrate using double-sided tape. Approximately 0.3 cm^3 of an aqueous suspension of the monodisperse polystyrene spheres diluted with water to 0.5 wt% was spread over the area of the substrate surrounded by the Teflon ring (0.785 cm^2)—this is enough material to form a template layer about 20 μm thick. The sample was then left undisturbed in a saturated humidity chamber to allow the spheres to sediment over a period of 3 to 4 days. Once the spheres had settled, a clear water layer appeared on top of the deposit. This water layer was then allowed to slowly evaporate over a period 3–4 days. Once all of the water had evaporated, the Teflon ring was removed to leave a circular area covered by the template. At this point, the template appears opalescent, as expected, with colours from green to red (depending on the angle of observation) clearly visible when the samples were illuminated from above with white light. The templates are robust and adhere well to the gold substrates and there is no evidence of re-suspension of the particles when they are placed in contact with the deposition solutions.

Synthesis of nanostructured macroporous lead oxides films

The electrochemical deposition of α-PbO_2 films was carried out at 0.90 V *vs.* SCE from a solution of 0.1 mol dm^{-3} lead acetate and 1.0 mol dm^{-3} sodium acetate (pH 5.5). β-PbO_2 films were deposited galvanostatically at 4.8 mA cm^{-2} from a solution of 0.1 mol dm^{-3} lead nitrate and 1.0 mol dm^{-3} nitric acid. Immediately prior to the deposition, the solutions were sparged with argon for 1 h to displace dissolved oxygen. Macroporous films used in SEM characterisation were grown with a gradient in thickness ranging from 0 to 1.5 μm across the 1 cm diameter sample. This was done in order to allow a systematic study by SEM of the surface topography as a function of the film thickness. The uniform gradient in film thickness was simply achieved by allowing the plating solution to slowly drain during deposition from a tap in the bottom of the cell whilst holding the substrate electrode vertical. After the deposition was complete (typically between 15 to 20 min), the films were soaked in toluene for 24 h to completely dissolve the polystyrene template. All experiments were performed at room temperature (20–23 °C).

Results and discussion

Electrochemical synthesis of α-PbO_2 from lead acetate solution

The macroporous α-PbO_2 film deposited from pH 5.5 solution through a 750 nm diameter template was dark red in colour, mechanically robust and chemically stable. When illuminated with white light, diffractive colours from green to red could be readily seen as the angle of observation was changed. Fig. 1 shows a set of SEM images for different thicknesses of the resulting film. Although the surface topography of the α-PbO_2 film changes as the film thickness changes, it is clear that the

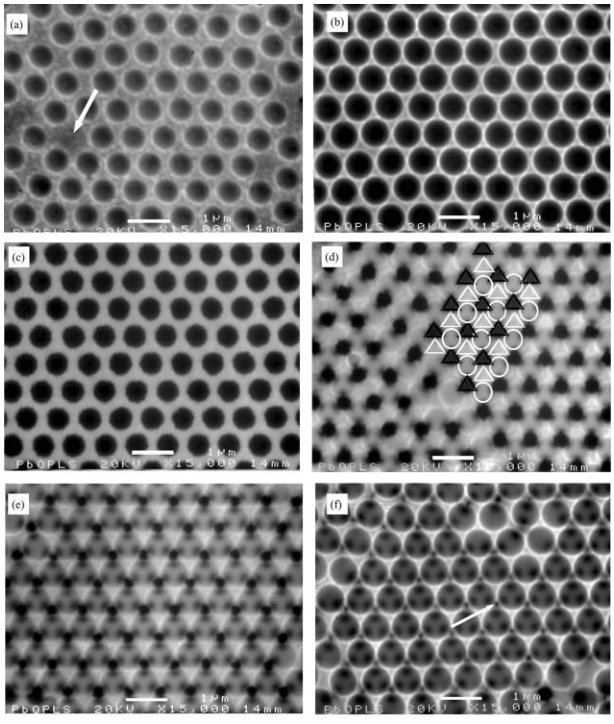

Fig. 1 SEM images of a macroporous α-PbO_2 film grown with a thickness gradient from 0.1 mol dm^{-3} $Pb(OAc)_2$ and 1.0 mol dm^{-3} NaOAc at 0.90 V *vs.* SCE through a template of 750 nm diameter polystyrene spheres. The estimated film thickness, based on the diameters of the mouths of the pores, are (a) 105, (b) 240, (c) 685, (d) 725, (e) 735 and (f) 857 nm. In every case, the scale bar is 1.0 μm.

highly ordered close-packed structure of the original spheres is faithfully preserved in the resulting α-PbO_2 film. The pore centre to pore centre distance estimated from the images (750 ± 30 nm) is in good agreement with the diameter of the polystyrene spheres used to form the template. Fig. 1(a) and (b) show images of a thinner part (thickness less than the template sphere radius) of the film. The pore mouth diameters estimated from the images are 520 and 700 nm, respectively. Based on these pore mouth diameters, we calculate film thicknesses of 105 and 240 nm for these two regions of the film. Although there are some defects in the packing of the pores [such as that indicated by the arrow in Fig. 1(a), which originates from a missing sphere in the original template], the α-PbO_2 deposited into the spaces between the spheres is smooth and uniform. Moreover, we can see that the pore mouths are circular in shape. Fig. 1(c) shows a part of the film where the thickness is greater than the template sphere radius. The pore mouths at this stage have a rounded hexagonal shape with an average pore diameter of about 410 nm. The estimated film thickness at this region is 685 nm.

With increasing film thickness, and because of the geometry of the packing of the spheres in the template, the film begins to grow around the spheres in the second layer, Fig. 1(d). This is apparent from the dark triangles and the spherical pores which correspond to the under layer and the upper layer of pores, respectively. This is made clearer in the figure by the black triangles and white circles superimposed on the image to represent the positions of the original template spheres in the lower and upper layers. The rounded triangular pore mouths (black triangles) have diameters of around 260 nm, whereas the spherical pores in the top layer (white circles) have average diameters of 540 nm. The estimated film thickness in this region is 725 nm. Note that the bright triangular areas in the image (indicated by the white triangles superimposed on the image), corresponding to the highest points of the oxide film, grow up from the underlying substrate through the interstices between the two bottom layers of template spheres. This type of complex surface topography has been observed for metal films prepared using the same method and is discussed in detail elsewhere.[16] It arises because of the interplay between the electrochemical growth of the film surface out from the electrode and the hindered diffusion of reactants to the growing surface. As a consequence, the surface of the growing film is not planar and these surface topographic features repeat, once the film is more than half the sphere diameter thick, as the film grows through successive layers of template spheres.

The SEM images in Fig. 1(e) and (f) show the three-dimensional structure of the α-PbO_2 film. In these two images, each large cavity in the top layer contains three small pores (diameter 80 ± 20 nm), seen as dark circles in the image. These small pores are the internal windows between the large pores in each successive layer and they occur at those points where the original spheres were in contact. The average upper pore mouth diameters in these two images are 610 and 670 nm, respectively, corresponding to film thicknesses in the two images of around 735 and 857 nm. Interestingly, although the film thickness in Fig. 1(f) is about 100 nm larger than the sphere diameter, there are still small voids, or spandrels [marked with an arrow in Fig. 1(f)], between the pores of the top layer of the film. These voids are filled in as the oxide film becomes thicker.

The SEM micrograph in Fig. 2(a) shows cross-sectional images of part of the film shown in Fig. 1. The film thickness in this region is about 450 nm and the film has a two-dimensional macroporous structure. Fig. 2(b) shows a cross-sectional image of a much thicker film deposited through a 500 nm diameter sphere template using a deposition charge of 1.0 C cm^{-2}. This image clearly shows that the pores embedded in the film form an ordered three-dimensional interconnected close-packed structure faithfully replicating the original arrangement of the template spheres. After correction for the tilt angle, the measured film thickness is 2.40 ± 0.10 μm. This measured thickness agrees well with the value (2.38 μm) calculated from the number of layers of pores (5.5 layers). For comparison, Fig. 2(c) shows a cross-sectional view of a non-templated α-PbO_2 film deposited under the same conditions with a deposition charge of 0.5 C cm^{-2}. In this case, the film is 600 nm thick, corresponding to a faradaic efficiency for the deposition process of 90%. The image shows that the film is both smooth and dense.

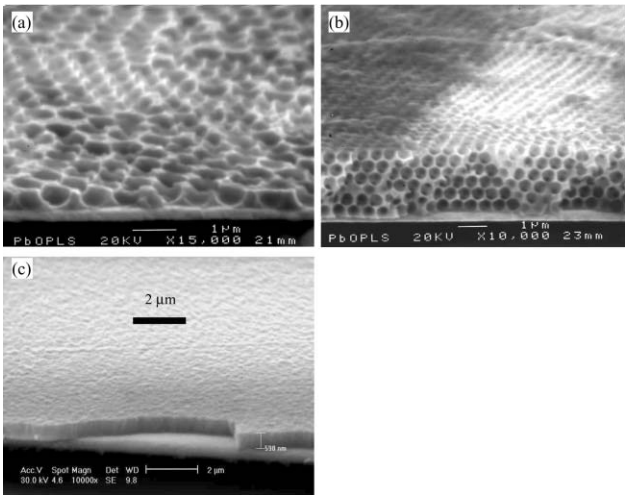

Fig. 2 Cross-sectional SEM images of α-PbO_2 films deposited on gold surfaces: (a) view of part of the film in Fig. 1, the film thickness in this region is 400 nm; (b) image of the edge of a cleaved α-PbO_2 film deposited at 0.90 V *vs.* SCE through a template made from 500 nm diameter polystyrene spheres using a charge of 1.0 C cm^{-2}; (c) image of a non-templated α-PbO_2 film deposited under identical conditions with a deposition charge of 0.5 C cm^{-2}, the film is about 600 nm thick.

The structure of the PbO_2 in the walls of the nanostructure was studied by X-ray diffraction, Fig. 3. The powder X-ray diffraction pattern clearly shows the characteristic reflections expected for highly polycrystalline orthorhombic α-PbO_2 with a strong (200) texture.[31] This structure is consistent with the crystal structure of non-templated electrodeposited α-PbO_2 films.[28,32,33] The average grain size of α-PbO_2 in the walls of the nanostructure, calculated from the width of the (200) diffraction peak at half maximum using the Scherrer equation[34] is 53 nm.

Electrochemical synthesis of macroporous β-PbO_2 from acidic solution

While α-PbO_2 is deposited from neutral or slightly acidic solutions, it is known that that β-PbO_2 can be deposited from

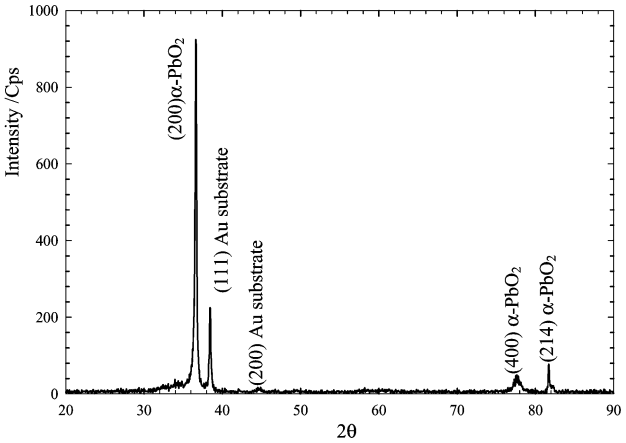

Fig. 3 Powder X-ray diffraction pattern for the macroporous α-PbO_2 film shown in Fig. 2(b).

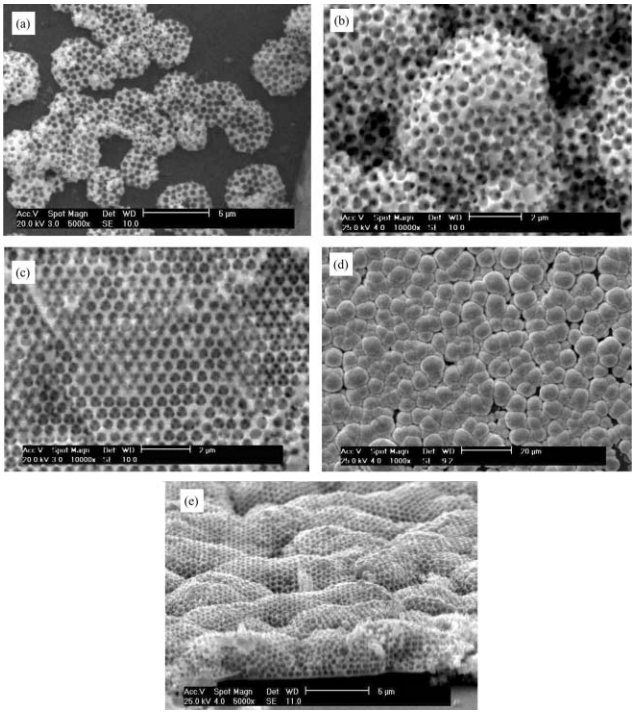

Fig. 4 SEM micrographs of macroporous β-PbO_2 deposited galvanostatically with a thickness gradient through a template of 500 nm polystyrene spheres on an ITO surface. The film was deposited from a solution of 0.1 mol dm^{-3} $Pb(NO_3)_2$ and 1.0 mol dm^{-3} HNO_3. (a), (b) and (c) show images with increasing film thickness, illustrating the development of the overlapping porous hemispherical structure into a complete film. (d) A non-templated β-PbO_2 film showing the characteristic overlapped granular structure. (e) Cross-sectional SEM image of a thick macroporous β-PbO_2 film.

acidic solution. Fig. 4 shows SEM micrographs of different parts of a macroporous β-PbO_2 film deposited with a thickness gradient through a template of 500 nm polystyrene spheres assembled on an ITO substrate. The image in Fig. 4(a) corresponds to one of the thinnest parts of the film. In the image, we can see a number of randomly distributed nearly hemispherical, overlapping structures, each punctuated by arrays of spherical pores, resulting in a honeycomb-like appearance. These hemispherical porous structures vary in size from 2.5 to 5 μm. Nevertheless, the pore centre to pore centre distances match the diameter of the original template spheres. On scanning across the film towards the thicker regions, we find that the hemispherical porous structures grow larger and eventually completely overlap, but that the surface does not become flat, Fig. 4(b). Because of the hemispherical shape of these porous structures, the spherical pores within them appear to be randomly packed. However, this is not the case and for the thickest β-PbO_2 film, when overlap is complete, the embedded pores show a highly ordered hexagonal close-packed structure, as shown in Fig. 4(c). Related electrochemical and SEM studies of the electrodeposition of non-templated β-PbO_2 indicate that in acid solution, the deposition proceeds *via* progressive three-dimensional nucleation and growth,[35] and this is entirely consistent with the structures described above. For comparison, Fig. 4(d) shows a non-templated β-PbO_2 film deposited under the same conditions. The micrograph shows the complete overlap of the nearly hemispherical β-PbO_2 structures, with sizes varying from about 2.0 to 5.0 μm. This is the same as is observed for the macroporous β-PbO_2 film. Again, the hemispherical shape of the granules in the deposit and the variation in their size is consistent with a progressive three-dimensional nucleation and growth mechanism.

Fig. 4(e) shows a cross-sectional image of a thicker part of the macroporous film. The image shows the three-dimensional close-packed structure of the uniform spherical pores, with the large overall variation in film thickness resulting from the growth mechanism.

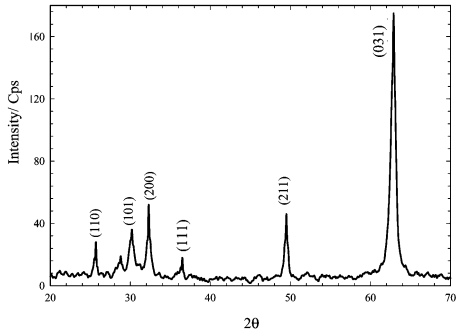

Fig. 5 Powder X-ray diffraction pattern of a macroporous β-PbO_2 film deposited from a solution of 0.1 mol dm^{-3} $Pb(NO_3)_2$ and 1.0 mol dm^{-3} HNO_3 at a constant current density of 4.8 mA cm^{-2} through a template of 500 nm diameter spheres assembled onto an ITO substrate.

Again, the structure of the PbO_2 in the walls of the nanostructure was confirmed using X-ray diffraction. Fig. 5 shows the powder X-ray pattern for the film shown in Fig. 4. The pattern shows the characteristic reflections expected for highly polycrystalline β-PbO_2 with a tetragonal structure and a preferred (031) orientation.[36] This structure is consistent with that obtained for non-templated films deposited under the same conditions.[37] The average grain size for the β-PbO_2 in the walls of the nanostructure was estimated to be 19 nm using the Scherrer equation.

Electrochemical behaviour of macroporous β-PbO_2 in sulfuric acid

β-PbO_2 is the active material on the cathode in fully charged lead acid batteries. In the discharge process, the β-PbO_2 is reduced in the presence of sulfuric acid to insoluble $PbSO_4$. During subsequent recharging, the $PbSO_4$ is converted back to PbO_2.[28] We were therefore interested to study the electrochemical behaviour of the macroporous β-PbO_2 films in 1.0 mol dm^{-3} H_2SO_4 to explore the effects of the nanostructure on the discharging and charging process and the stability of the structure upon cycling. For these experiments, the macroporous films were prepared from the acid electrolyte using a template assembled from 500 nm spheres on a 1 mm diameter Au electrode using a charge of 0.4 C cm^{-2}, corresponding to a film which is, on average, two pore layers thick. For comparison, a non-templated β-PbO_2 film was prepared on an identical 1 mm diameter Au electrode using the same deposition conditions.

Fig. 6 shows cyclic voltammograms of the two films recorded at 100 mV s^{-1} in 1 mol dm^{-3} H_2SO_4. In each case, the first cycle sweeping cathodic from 1.5 V is shown in Fig. 6(a). On scanning to more negative potentials, a well-defined reduction peak is observed at 1.25 V for both films. This is generally assigned to the reduction of β-PbO_2 to $PbSO_4$ according to the electrochemical reaction in eqn. 1.[28,29]

$$PbO_2\,(s) + HSO_4^-\,(aq) + 3H^+ + 2e^- \rightarrow PbSO_4\,(s) + 2H_2O \quad (1)$$

Although the two electrodes have the same amount of β-PbO_2 deposited on them, the charge passed for the macroporous β-PbO_2 electrode (as determined from the area under the cathodic peak) is about 7 times larger than that for the non-templated film. This is consistent with the expected increase in surface area for the macroporous film. On the reverse scan, for both films, only relatively small anodic peaks are seen (the ratio of the charges between the anodic and cathodic peaks is about 10% in both cases), showing that the

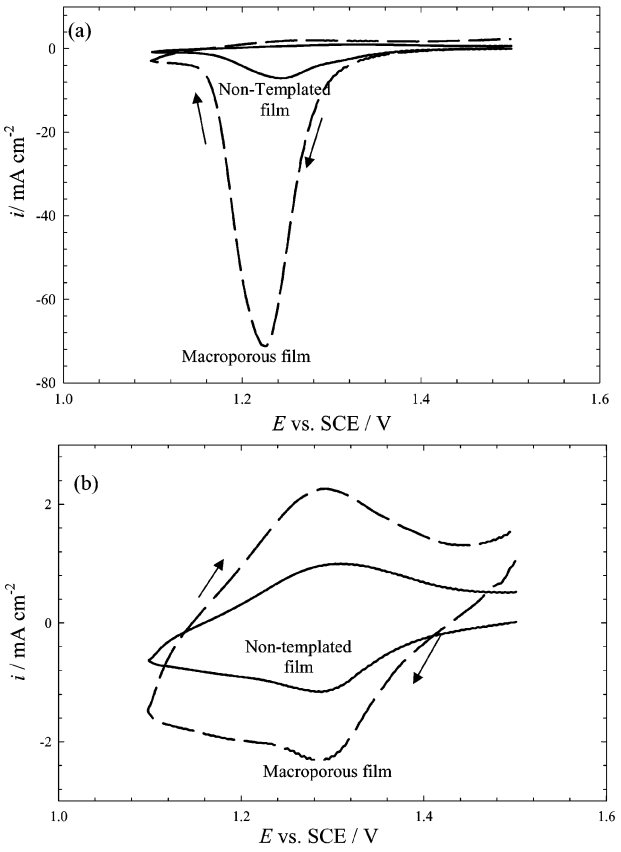

Fig. 6 Cyclic voltammograms of templated (500 nm pore diameter) and non-templated β-PbO_2 films in 1 mol dm^{-3} H_2SO_4 recorded a scan rate of 100 mV s^{-1}. Both films were electrodeposited from a solution of 0.1 mol dm^{-3} $Pb(NO_3)_2$ and 1.0 mol dm^{-3} HNO_3 at a current density of 4.8 mA cm^{-2} with a total charge of 0.4 C cm^{-2} on 1 mm diameter Au disk electrodes: (a) the first cycle; (b) the tenth cycle.

re-oxidation of $PbSO_4$ to PbO_2 is a slow process.[28] The results indicate that about 90% of the $PbSO_4$ produced is not converted back to PbO_2. This is consistent with the known passivating effect of $PbSO_4$.[28] As a result, on the next cycle, the cathodic peak is much smaller since there is less PbO_2 available for reduction. With repeated cycling, the charges for the anodic and cathodic processes become equal. Nevertheless, after 10 cycles, the charge passed at the macroporous electrode is still about twice that passed at the non-templated electrode, as shown in Fig. 6(b).

After cycling in sulfuric acid, the surface topography of the macroporous β-PbO_2 film was characterised using SEM. Fig. 7 shows micrographs for a macroporous β-PbO_2 film prepared using a 750 nm sphere template after 10 cycles in 1 mol dm^{-3} sulfuric acid. The micrographs show that the ordered spherical pores that were originally embedded in the PbO_2 have been significantly filled up on cycling in acid [compare this image to that in Fig. 4(c)]. Nevertheless, the pore centre to pore centre distance still matches the diameter of the original template spheres. In addition, the Fourier transform of the image, shown in the inset of Fig. 7(a), confirms the presence of long-range hexagonal order. From these observations, we conclude that the basic close-packed structure of the pores within the film remains, but that the spherical shape of the pores has been distorted by the significant expansion and contraction of the surface of the material accompanying the electrochemical conversion of β-PbO_2 to $PbSO_4$ and back (the molar volumes of β-PbO_2 and $PbSO_4$ are 25.5 and 49.2 cm^3 mol^{-1}, respectively[38]) and as a result of the fact that about 90% of the $PbSO_4$ produced on the first cathodic cycle is not converted back to PbO_2 on the return cycle and, therefore, must remain on the surface of the film.

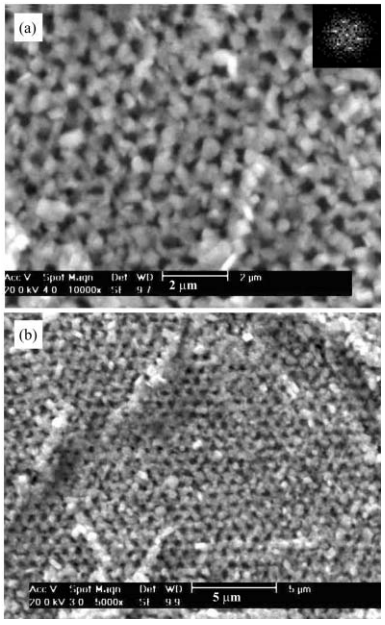

Fig. 7 SEM micrographs of a macroporous β-PbO_2 film after ten cycles in 1 mol dm^{-3} H_2SO_4. The film was electrodeposited on an ITO surface through a template of 750 nm diameter spheres from a solution of 0.1 mol dm^{-3} $Pb(NO_3)_2$ and 1.0 mol dm^{-3} HNO_3 at a constant current density of 4.8 mA cm^{-2} and with a total charge passed of 0.4 C cm^{-2}: (a) high magnification (the inset shows a Fourier transform of the image); (b) low magnification image.

Conclusions

We have shown that highly ordered macroporous films of both α-PbO_2 and β-PbO_2 can be prepared by electrodeposition through templates assembled from sub-micron diameter polystyrene spheres assembled on either gold or ITO substrates. The presence of the template does not alter the nucleation mechanism or the polymorph of PbO_2 deposited as confirmed by scanning electron microscopy and X-ray diffraction characterisation. The electrochemical activity of the macroporous β-PbO_2 as measured from the change passed in the conversion to $PbSO_4$ on cycling in H_2SO_4 is larger than that for the corresponding non-templated film due to the greater surface area. As a result of the significant volume change accompanying the electrochemical conversion of β-PbO_2 to or from $PbSO_4$, the macroporous structure of the β-PbO_2 is significantly degraded after a few redox cycles in H_2SO_4.

Acknowledgements

M. A. G. thanks the Embassy of the Arab Republic of Egypt, London, for financial support and we thank Mr A Clark for assistance with SEM.

References

1 S. J. Sarrade, G. M. Rios and M. Carles, *Sep. Purif. Technol.*, 1998, **14**, 19.
2 P. Diddams and K. Smith, *Inorganic Supports and Catalysts*, Ellis Horwood, Chichester, 1992.
3 T. J. Clough, *US Pat.*, 5895732, 1999.
4 J. E. G. J. Wijnhoven and W. L. Vos, *Science*, 1998, **281**, 802.
5 H. Yan, C. F. Blandford, B. T. Holland, W. H. Smyrl and A. Stein, *Chem. Mater.*, 2000, **12**, 1134.
6 B. T. Holland, C. F. Blandford, T. Do and A. Stein, *Chem. Mater.*, 1999, **11**, 795.
7 B. T. Holland, L. Abrams and A. Stein, *J. Am. Chem. Soc.*, 1999, **121**, 4308.
8 B. T. Holland, C. F. Blandford and A. Stein, *Science*, 1998, **281**, 538.
9 H. Yan, C. F. Blandford, J. C. Lytle, C. B. Carter, W. H. Smyrl and A. Stein, *Chem. Mater.*, 2001, **13**, 4314.

10 P. V. Braun and P. Wiltzius, *Nature*, 1999, **402**, 603.
11 J. E. G. J. Wijnhoven, S. J. M. Zevenhuizen, M. A. Hendriks, D. Vanmaekelbergh, J. J. Kelly and W. L. Vos, *Adv. Mater.*, 2000, **12**, 888.
12 L. Xu, W. L. Zhou, C. Frommen, R. H. Baughman, A. A. Zakhidov, L. Malkinski, J. Q. Wang and J. B. Wiley, *Chem. Commun.*, 2000, 997.
13 P. N. Bartlett, P. R. Birkin and M. A. Ghanem, *Chem. Commun.*, 2000, 1671.
14 T. Sumida, Y. Wada, T. Kitamura and S. Yanagida, *Chem. Commun.*, 2000, 1613.
15 P. N. Bartlett, P. R. Birkin, M. A. Ghanem and C.-S. Toh, *J. Mater. Chem.*, 2001, **11**, 849.
16 P. N. Bartlett, J. J. Baumberg, P. R. Birkin, M. A. Ghanem and M. C. Netti, *Chem. Mater.*, 2002, **14**, 2199.
17 T. Sumida, Y. Wada, T. Kitamura and S. Yanagida, *Chem. Lett.*, 2001, 38.
18 T. Sumida, Y. Wada, T. Kitamura and S. Yanagida, *Chem. Lett.*, 2002, 180.
19 D. Pletcher and F. C. Walsh, *Industrial Electrochemistry*, Chapman and Hall, London, 1990.
20 L. A. Larew, J. S. Gordon, Y.-L. Hsiao and D. C. Johnson, *J. Electrochem. Soc.*, 1990, **137**, 3071.
21 A. M. Polcaro, S. Palmas, F. Renoldi and M. Mascia, *J. Appl. Electrochem.*, 1999, **29**, 147.
22 S. Stucki, G. Theis, R. Kötz, H. Devantay and H. J. Christen, *J. Electrochem. Soc.*, 1985, **132**, 367.
23 W. R. LaCourse, Y. L. Hsiao, D. C. Johnson and W. H. Weber, *J. Electrochem. Soc.*, 1989, **136**, 3714.
24 N. B. Tahar and A. Savall, *J. New Mater. Electrochem. Syst.*, 1999, **2**, 19.
25 J. Grimm, D. Bessarabov, W. Maier, S. Storck and R. D. Sanderson, *Desalination*, 1998, **115**, 295.
26 C. N. Ho and B. J. Hwang, *Electrochim. Acta*, 1993, **38**, 2794.
27 T. C. Wen, M. G. Wei and K. L. Lin, *J. Electrochem. Soc.*, 1990, **137**, 2700.
28 M. E. Herron and D. Pletcher, *J. Electroanal. Chem.*, 1992, **332**, 183.
29 D. Velayutham and M. Noel, *Electrochim. Acta*, 1991, **36**, 2031.
30 N. Munichandraiah, *J. Appl. Electrochem.*, 1992, **22**, 825.
31 *Diffraction Data*, PCPDFWIN version 2.01, JCPDS-International Centre for Diffraction Data, Philadelphia, PA, USA, 1998, file no. 72-2102.
32 T. Wen, M. Wei and K. Lin, *J. Electrochem. Soc.*, 1990, **137**, 2700.
33 C. N. Ho and B. J. Hwang, *Electrochem. Acta*, 1993, **38**, 2749.
34 C. Hammond, *The Basics of Crystallography and Diffraction*, Oxford University Press, Oxford, 1997.
35 J. González-Garc, F. Gallud, J. Iniesta, V. Montiel, A. Aldaz and A. Lasia, *J. Electrochem. Soc.*, 2000, **147**, 2969.
36 *Diffraction Data*, PCPDFWIN version 2.01, JCPDS-International Centre for Diffraction Data, Philadelphia, PA, USA, 1998, file no. 37-0517.
37 J. Lee, H. Varela, S. Uhm and Y. Tak, *Electrochem. Commun.*, 2000, **2**, 646.
38 R. C. Weast, in *CRC Handbook of Chemistry and Physics*, ed. D. R. Lide, CRC Press, Boca Raton, FL, 65th edn., 1985, B107.